CHAPTER V

RESULTS AND DISCUSSION

The nanocrystalline titanium dioxide (titania) obtained in this work were synthesized from Titanium tert-butoxide (TTB) mixed with organic solvents, 1,4 butanediol or toluene, in an autoclave under autogenous pressure. The procedure is the so-call solvothermal method. Titania prepared in each organic solvent have different physical properties and thermal stability (Sornnarong Theinkaew, 2000: 70).

5.1 Formation of dioxide

5.1.1 Synthesis of titanium dioxide in 1,4-butanediol

Titanium dioxide has been synthesized in 1,4-BG at various conditions (Glycothermal Method). Under glycothermal conditions, titanium (IV) tert-butoxide (TTB) was easily converted to glycoxide. Thermal decomposition of the glycoxide molecule was occurred by intramolecular participation of the remaining hydroxyl group of glycol moiety and subsequently a $\equiv Ti\text{-}O^-$ anion was formed. The nucleophilic attack of this titanate ion on another ion and crystallization of titanium (IV) oxide were taken place.

The as-synthesized nanocrystalline titania products that crystallite sizes are 10, 13, and 17 nm were synthesized by reaction in 1,4-BG at various condition as show in Table 5.1. XRD patterns indicated that the as-synthesized products were the anatase phase for all of the products as shown in Figure 5.1. These confirmed that the reaction yielded the anatase titania products and non-contaminate with other phases such as brookite or rutile.

The titania products were characterized by SEM for analyzing morphology of the products as shown in Figure 5.2. SEM results indicate that morphology of the secondary particle which a shape was irregular particle is not change with increasing the reaction time.

Table 5.1 shows the crystallite sizes calculated from XRD patterns at the 101 diffraction peak of anatase titania by Scherrer equation and the specific surface area of titania by BET measurement. For holding the reaction time 2 hr, the crystallite size and BET surface area of the as-synthesized product were 10 nm and 139 m^2/g, respectively. Alternatively, the surface area which was calculated from diameter of the crystal became 154 m^2/g. It was noted that the equation was used to calculate as $6/d\rho$ on assumption that the crystal is nonporous spherical crystal (Kominami *et al.*, (1999). Interestingly, the obtained surface area was not different from BET surface area. These identify that the titania product is not contaminate with amorphous-like phase or organic phase as shown through ratio of S_1/S_2 in Table 5.1 (S_1 is BET surface area and S_2 is surface area calculated). Kominami *et al.* (1997) synthesized TiO_2 from the solvothermal method. They calculated the surface area from the crystallite size by assuming the density of anatase to be 3.9 g cm^{-3}. They found that the surface area obtained from BET measurement was larger than that calculated from the crystallite size and suggested that the product was contaminated with the amorphous-like phase.

For other reaction times, the approximate unity of S_1/S_2 ratio implied that the products were without the amorphous phase. When the reaction time was increased, the specific surface area decreased but the crystallite size increased slightly.

Table 5.1 Crystallite size and surface area of titania products synthesized in 1,4-BG.

Crystallite size (nm)	*Reaction temperature (°C)*	*Reaction time (hr)*	*Reactant concentration (g/100ml)*	*Surface area (m^2/g)*		*S_1/S_2*
				S_1 [a]	*S_2* [b]	
10	300	2	7.5	139	154	0.9
13	300	2	15	110	118	0.9
17	320	4	25	90	94	1.0

[a] Specific BET surface area from BET measurement.

[b] Specific surface area calculated from equation of $6/d\rho$ on assumption that the crystal is spherical particle and the density of anatase titania is 3.9 g cm^{-3}.

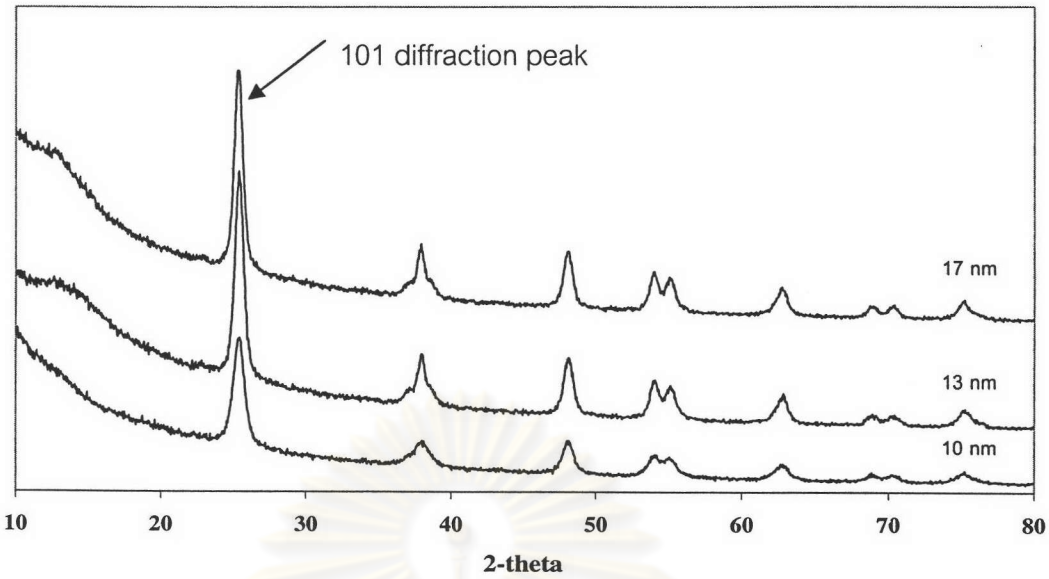

Figure 5.1 XRD patterns of titania product that synthesized in 1,4-BG for various condition.

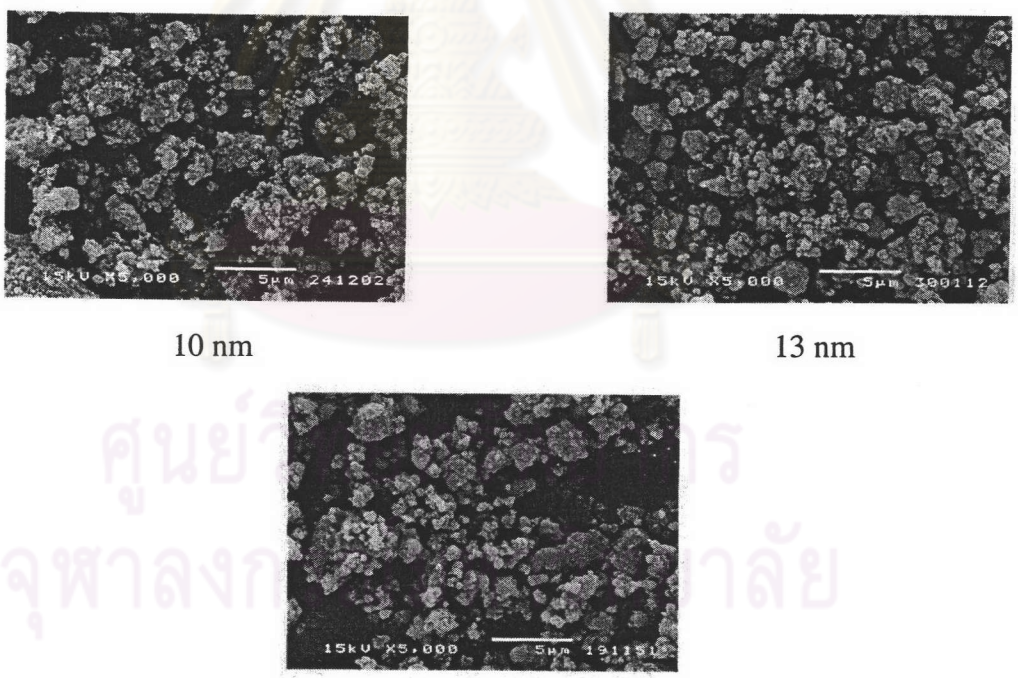

10 nm 13 nm

17 nm

Figure 5.2 SEM morphology of titania products synthesized in 1,4-BG for various condition.

Table 5.2 shows pore volumes and average pore diameters of the titania products for various condition.

Table 5.2 Pore volume and average pore diameter of titania products synthesized in 1,4-BG for various reaction time.

Crystallite size (nm)	*Reaction temperature (℃)*	*Reaction time (hr)*	*Reactant concentration (g/100ml)*	*Pore volume (cc/g)*[a]	*Average pore diameter (nm)*[b]
10	300	2	7.5	0.4	12
13	300	2	15	0.4	11
17	320	4	25	0.4	12

[a] BJH cumulative desorption pore volume of pores

[b] BJH desorption average pore diameter (4V/A)

5.1.2 Synthesis of titanium dioxide in toluene

Titanium dioxide has been synthesized in toluene at various conditions (Solvothermal Method). Under inert organic solvent condition, thermal decomposition of TTB in toluene was occurred, yielding a ≡Ti-O^- anion. The nucleophilic attack of the titanate ion on another ion and crystallization was taken place, finally yielding the anatase titania.

Titania was synthesized for various conditions as shown in Table 5.3. From XRD patterns, the crystallite size of the anatase samples was calculated from the half-height width of the 101 diffraction peak of anatase using the Scherrer equation.

Table 5.3 Crystallite size and surface area of TiO_2 products synthesized in toluene

Crystallite size (nm)	*Reaction temperature (℃)*	*Reaction time (hr)*	*Reactant concentration (g/100ml)*	*Surface area (m^2/g)*		*S_1/S_2*
				S_1[a]	*S_2*[b]	
10	300	0.5	15	156	154	1.0
13	300	2	25	120	118	1.0
17	320	6	25	91	94	1.0

[a] Specific BET surface area from BET measurement.

[b] Specific surface area calculated from equation of 6/dρ on assumption that the crystal is spherical particle and the density of anatase titania is 3.9 g cm^{-3}.

Table 5.4 shows the pore volume and the average pore diameter of TiO_2 products synthesized in toluene for various conditions.

Table 5.4 Pore volume and average pore diameter of titania product synthesized in toluene.

Crystallite size (nm)	*Reaction temperature (℃)*	*Reaction time (hr)*	*Reactant concentration (g/100ml)*	*Pore volume (cc/g)*[a]	*Average pore diameter (nm)*[b]
10	300	0.5	15	0.3	4
13	300	2	25	0.3	6
17	320	6	25	0.3	7

[a] BJH cumulative desorption pore volume of pores

[b] BJH desorption average pore diameter (4V/A)

The XRD patterns of the products prepared in different condition are given in Figure 5.3. The relevant SEM micrographs of products are shown in Figure 5.4.

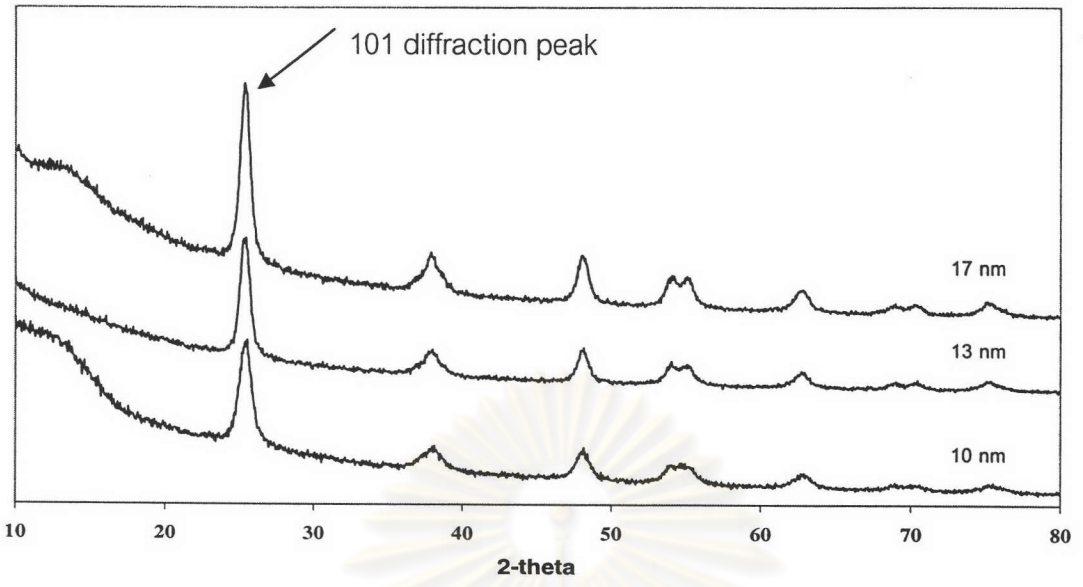

Figure 5.3 XRD patterns of titania product that synthesized in toluene for various condition.

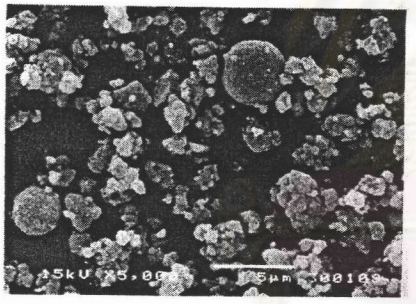

10 nm

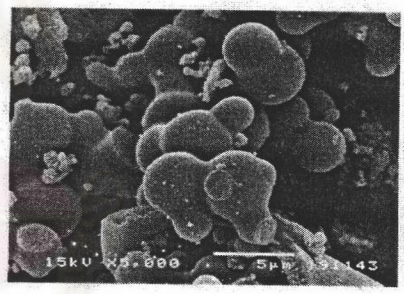

13 nm

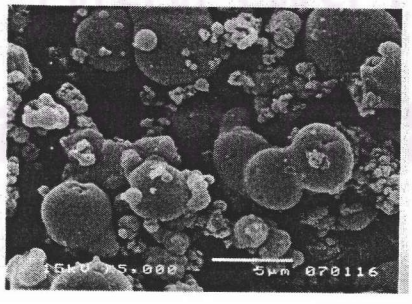

17 nm

Figure 5.4 SEM morphology of titania products synthesized in toluene for various condition.

5.2 Photocatalysis reaction

5.2.1 Photocatalytic decomposition of ethylene by using different crystallite size catalysts

In this study, the catalysts used are TiO_2 synthesized by solvothermal method as shown in Tables 5.1 and 5.3. Figure 5.5 shows the profiles of conversion of ethylene using three crystallite size catalysts and compare between catalysts synthesized by different solvent during photocatalytic decomposition of 1000 ppm ethylene. The flow rate of air was set at 10 ml/min. The photocatalytic reaction operated at room temperature. After switching on the UV lamp of the reactor, photocatalytic reaction started.

The first 60 minutes of running is the waiting time for system to prepare surface catalyst by feeding of air and irradiation were conducted. After the feeding of ethylene, the conversion of ethylene increases up to the highest conversion and decreases to the conversion at the steady state for 300 minutes operation time. The increase of conversion to the highest value in the initial period operation time due to the amount of species adsorbed on catalyst surface was at the saturated value. After that, a decrease conversion is observed due to the amount of species adsorbed on catalyst surface was decreased. Then, the conversion at the final time of operation was nearly constant due to the equilibrium between the adsorption of gaseous on the catalyst surface and the consumption of surface species (Park *et al.*,1999).

UV irradiation of several standard TiO_2 catalysts in the presence of C_2H_4 and O_2 led to the oxidation of C_2H_4 to produce CO_2, CO, and H_2O as the main products, but with relative reactivity and selectivity, depending on the specific properties of the catalysts.

When TiO_2 is illuminated by the light of energy greater than the band gap, e^- and h^+ are generated. The e^- and h^+ need to diffuse to catalyst surface where they are captured by electron and hole acceptors. Water and O_2 molecules adsorbed on surface catalyst are captured with e^- and h^+ and then produced $^{\cdot}OH$ and $O_2^{\cdot-}$, respectively.

Both ·OH and $O_2^{\cdot-}$ are the active radicals to take a part in the chain reaction with organic compounds and then the organic compounds are degraded.

The observed photocatalytic conversions were in the order of crystallite size 17>13>*10* nm in both solvents. The crystal grows in size and the surface structure may be altered, such as surface defects and bulk defects. Surface defects are good for high photoactivity because they are used as an active site on which the electron donor or acceptor is adsorbed. However, the bulk defect lowers the photoactivity because they provide sites for the recombination of the photogenerated electrons (Howe *et al.*, 1985; Howe *et al.*, 1987; Nakaoka *et al.*, 1997).

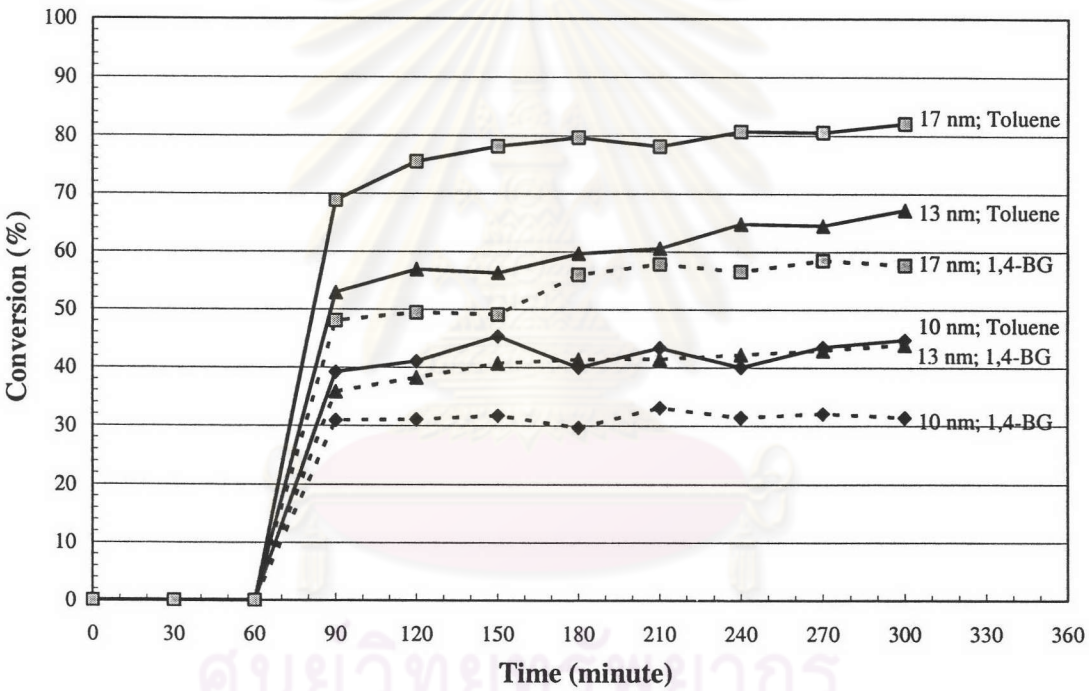

Figure 5.5 Time course of conversion in the photocatalytic decomposition of ethylene over TiO_2 synthesized by solvothermal method.

From Figure 5.5, the change of photocatalytic conversions depended on crystallite size, the photocatalytic conversions were dramatically increased if the crystallite size was increased. But Zhang *et al* (2000) have reported that the reduction of the bulk defect and the increase of crystallinity of anatase phase with the heat treatment, which crystallite size increase and surface area decrease, does increasing the photocatalytic efficiency. Figure 5.6 shows the time course of conversion in the

photocatalytic decomposition of ethylene on TiO_2 catalysts with crystallite sized 10 nm as-synthesized and heated at 300°C for 2 h TiO_2 catalysts.

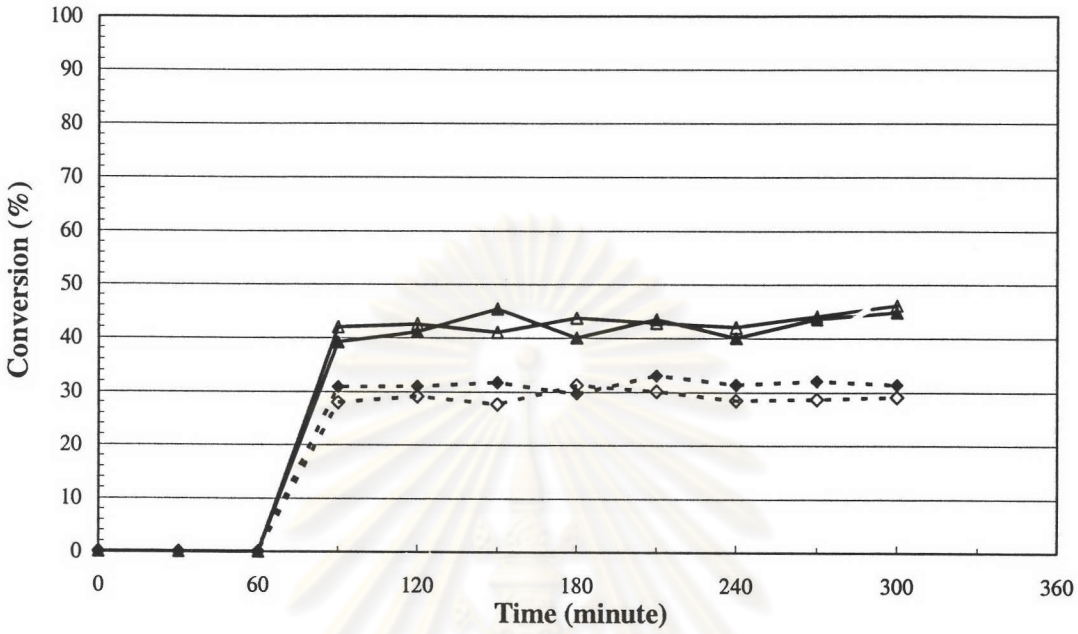

Figure 5.6 Time course of conversion in the photocatalytic decomposition of ethylene on as-synthesized (♦) 10 nm in 1,4-BG (▲) 10 nm in toluene and calcined at 300°C for 2 h (◊) 10 nm in 1,4-BG (Δ) 10 nm in toluene TiO_2 catalysts.

From Figure 5.6, the photocatalytic conversions of as-synthesized and heated at 300°C for 2 h TiO_2 catalysts are not different. We have attributed that the heat treatment resulting in the production of anatase phase of high crystallinity and effectively reducing the bulk defects that serve as the recombination centers is not effect on photocatalytic conversions. Then, from Figure 5.6 indicated that the increase of photocatalytic conversions in this case did not depend on bulk defects. In addition, we have concluded that the increase of photocatalytic conversions in this case depended on surface defects, and indicated that surface defects were increased if the crystallite size was increased.

Thompson *et al* (2003) have reported that the thermal desorption of CO_2 from TiO_2 (110) can therefore be used as a tool to investigate defect production on TiO_2 (110) surfaces. Henderson (1998) has observed the characteristic two-step desorption process which is indicative of the presence of both vacancy defect (Ti^{3+}) and

nondefective (Ti^{4+}) TiO_2 sites on surface. And anion vacancy defect sites are important in the application of TiO_2 to photooxidation chemistry, since O_2 reactant is preferentially adsorbed on these sites (Henderson *et al*, 1999).

CO_2 temperature programmed desorption (TPD) of the prepared catalysts were conducted with the manual controller in the temperature range of -150°C to 0°C. Thermal conductivity detector of Gow Mac gas chromatography was used to detect the signal of CO_2 desorption. The results were shown in Figures 5.7-5.11.

From the CO_2 TPD result of the catalyst prepared in 1,4-BG and toluene at crystallite sizes 10, 13, and 17 nm (Figures 5.7 and 5.8), the TPD curve contained two desorption peaks at approximately -150°C and -86°C, respectively. The CO_2 feature seen at low temperature at about -150°C is attributed to CO_2 molecules that are bound to regular five-coordinate Ti^{4+} sites (Thompson *et al*, 2003). The appearance of the high temperature TPD feature (at about -86°C) as a shoulder to peak is attributed to CO_2 bound to the defective TiO_2 surface, specifically to oxygen vacancy site (Ti^{3+}). The developments of the area of a shoulder to peak for various crystallite sizes indicate that larger crystallite size have more surface defects.

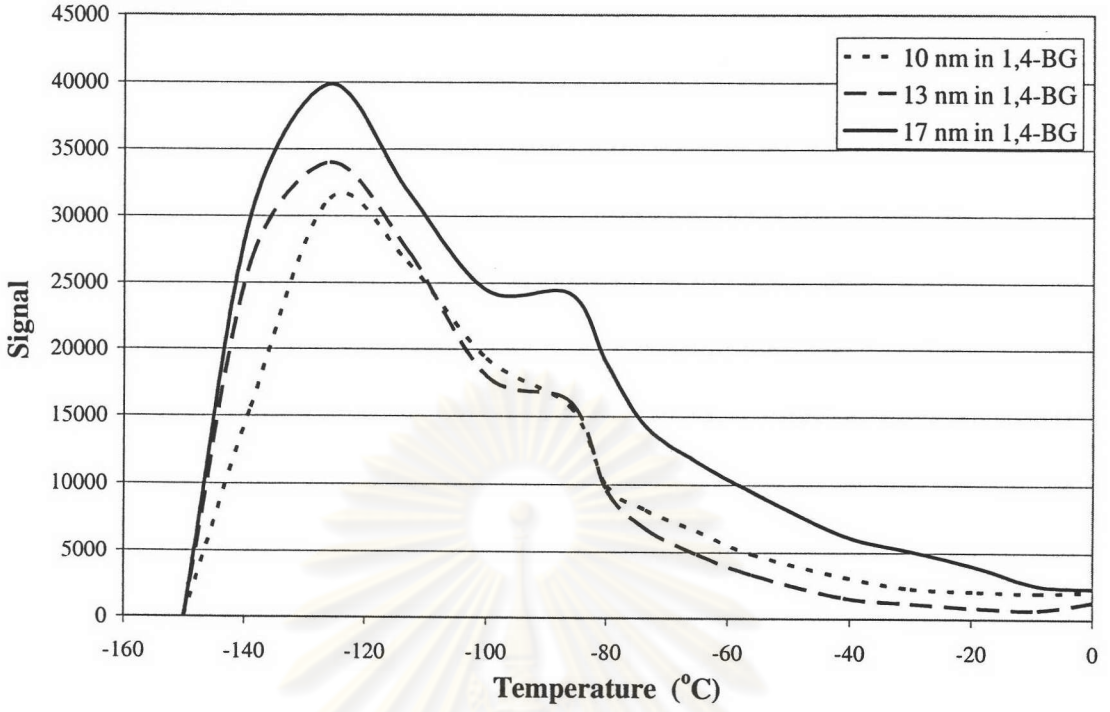

Figure 5.7 CO_2 TPD curve of prepared TiO_2 catalyst in 1,4-BG.

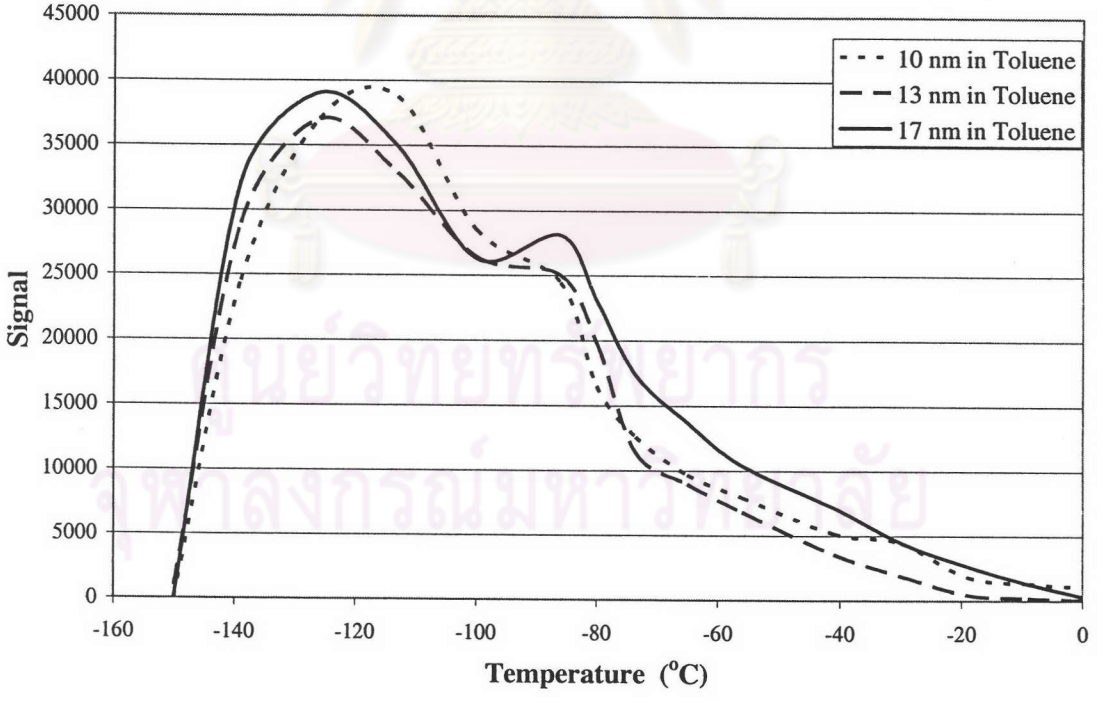

Figure 5.8 CO_2 TPD curve of prepared TiO_2 catalyst in toluene.

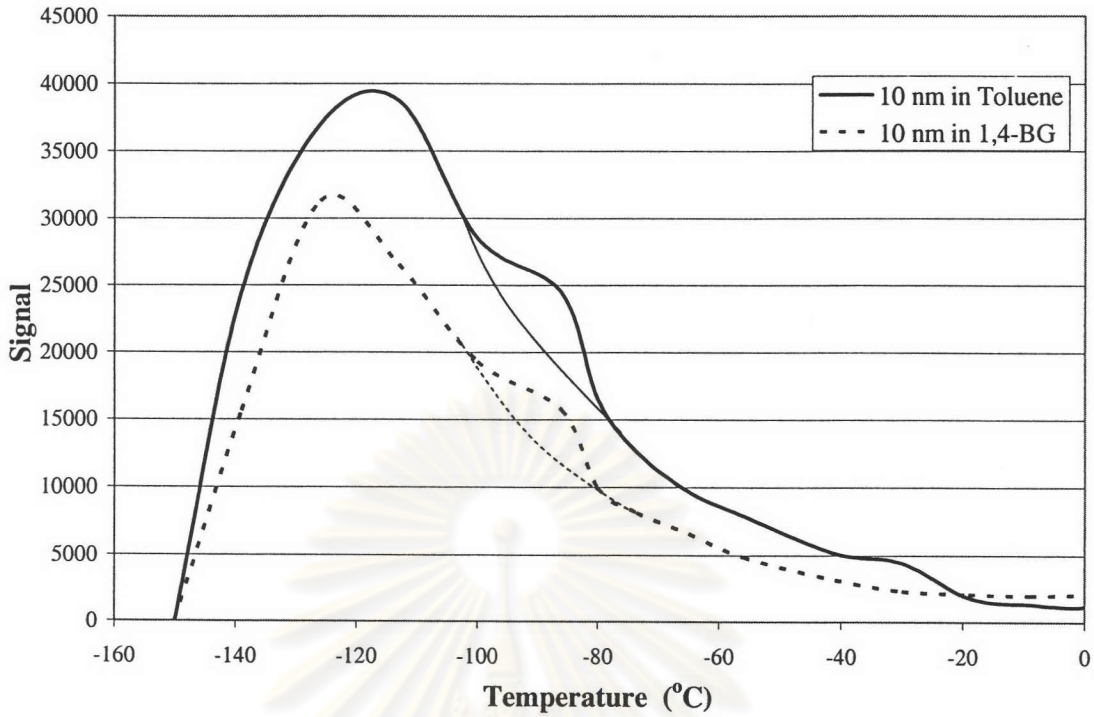

Figure 5.9 CO_2 TPD curve of TiO_2 catalyst crystallite size 10 nm.

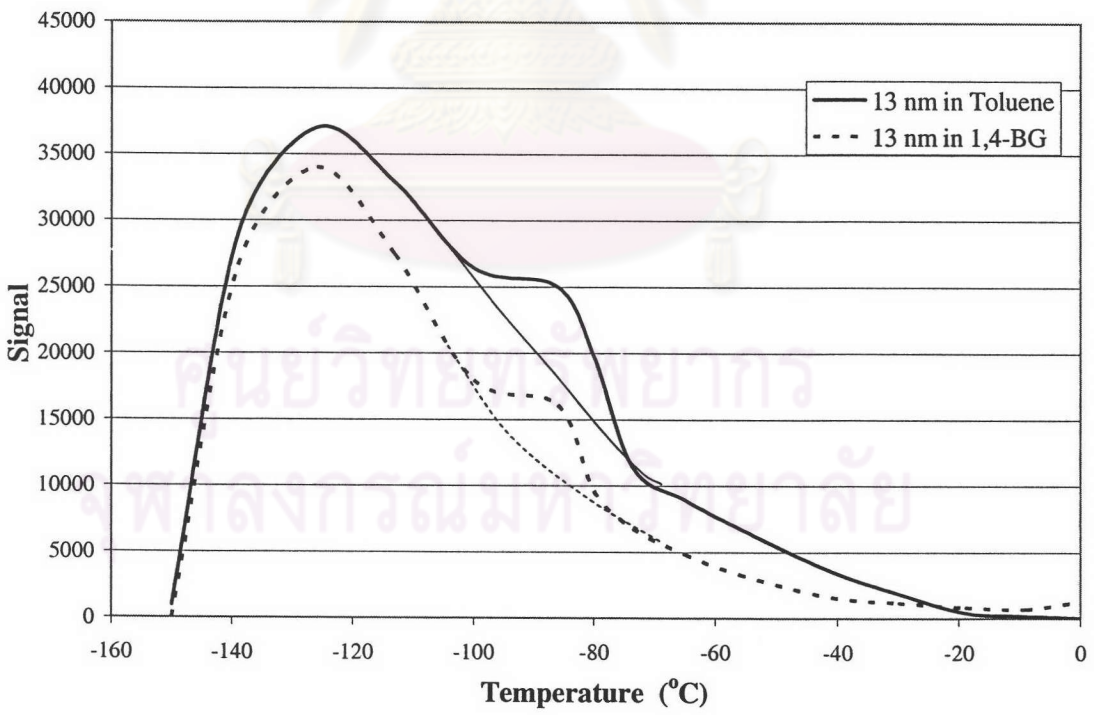

Figure 5.10 CO_2 TPD curve of TiO_2 catalyst crystallite size 13 nm.

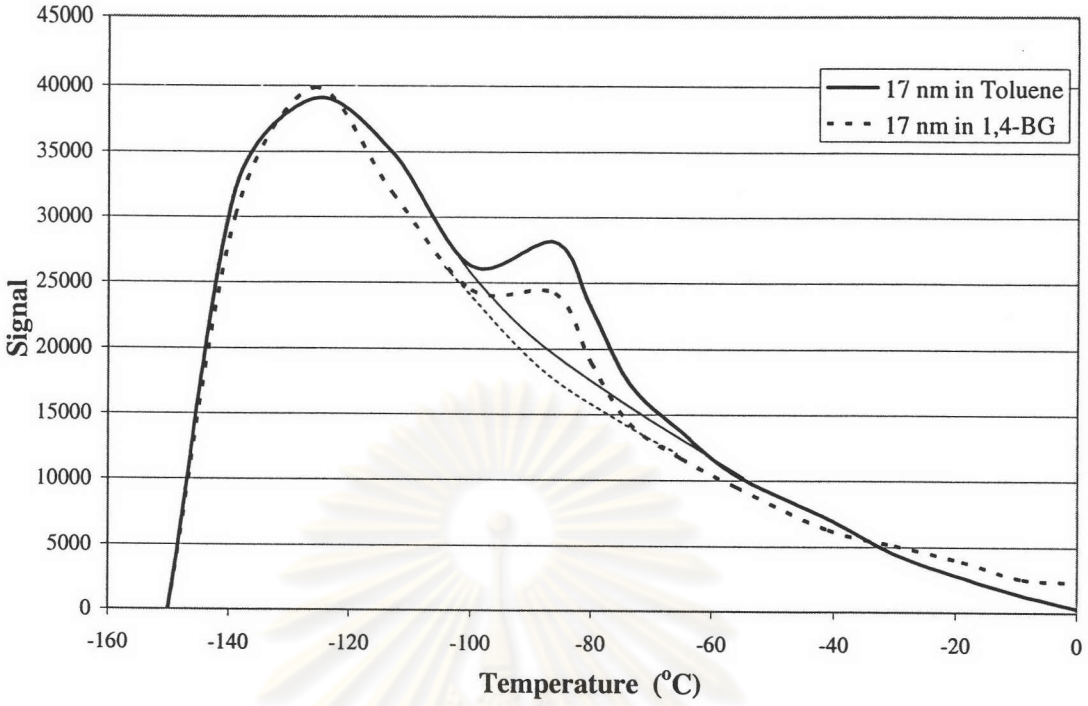

Figure 5.11 CO_2 TPD curve of TiO_2 catalyst crystallite size 13 nm.

5.2.2 Photocatalytic decomposition of ethylene on TiO_2 by using different solvents

In previous study, it was found that the mechanism of synthesized titania in 1,4-BG and the mechanism of synthesized titania in toluene are different (Wachiraphan, 2002).

The photocatalytic conversion of titanium dioxide powders synthesized in toluene was higher than titanium dioxide powders synthesized in 1,4-BG as shown in Figure 5.5. Because the mechanism of synthesized titanium dioxide in 1,4-BG was directly crystallization, but the mechanism of synthesized titanium dioxide in toluene proceeded via solid state reaction from precipitated amorphous (Wachiraphan, 2002). For the crystallization, the improvement of crystallinity and decrease of surface defects resulting from crystals are grown most slowly. But the solid state reaction from precipitated amorphous are those that growth most rapidly, increase surface defects. Crystal growth often follows the rough growth mechanism identified by irregular crystal surfaces. Precipitation is so fast that the building units of the crystal do not have enough time to adequately arrange themselves according to a

thermodynamically stable configuration, and a partially or fully amorphous product results.

Figures 5.9-5.11 shown the comparision TPD result of the catalyst prepared in 1,4-BG and toluene in the same size. We find that the area of a shoulder to peak of prepared TiO_2 catalyst in toluene more than the area of a shoulder to peak of prepared TiO_2 catalyst in 1,4-BG. And it indicates that prepared TiO_2 catalyst in toluene have more surface defects than prepared TiO_2 catalyst in 1,4-BG.

5.3 Effect of heating time and synthesized solvents on crystallite sizes

5.3.1 Heating time

XRD patterns of TiO_2 nano-powders heated at different temperatures are shown in Figures 5.12 and 5.13. The phase transformation from anatase to rutile occurred at about 900°C and completed at about 1020°C while in Wachiraphan's report (2002), the presence of the rutile was at about 900°C.

The effect of the heating time upon the crystallite size of TiO_2 powders is shown in Figures 5.14 and 5.15. At low heating temperatures the prolongation of heating time has little influence on the particle size as shown in Figure 5.14. But when the heating temperature increases to 1020 °C, the obvious influence upon crystallite size was found as shown in Figure 5.15. At relatively high temperatures the heating time seems to have greater effect upon the crystallite size. Just as shown in Figure 5.14 and Figure 5.15, when the heating temperatures are 800, 1020°C the total crystallization had been completed and the corresponding phase type is anatase and rutile, respectively.

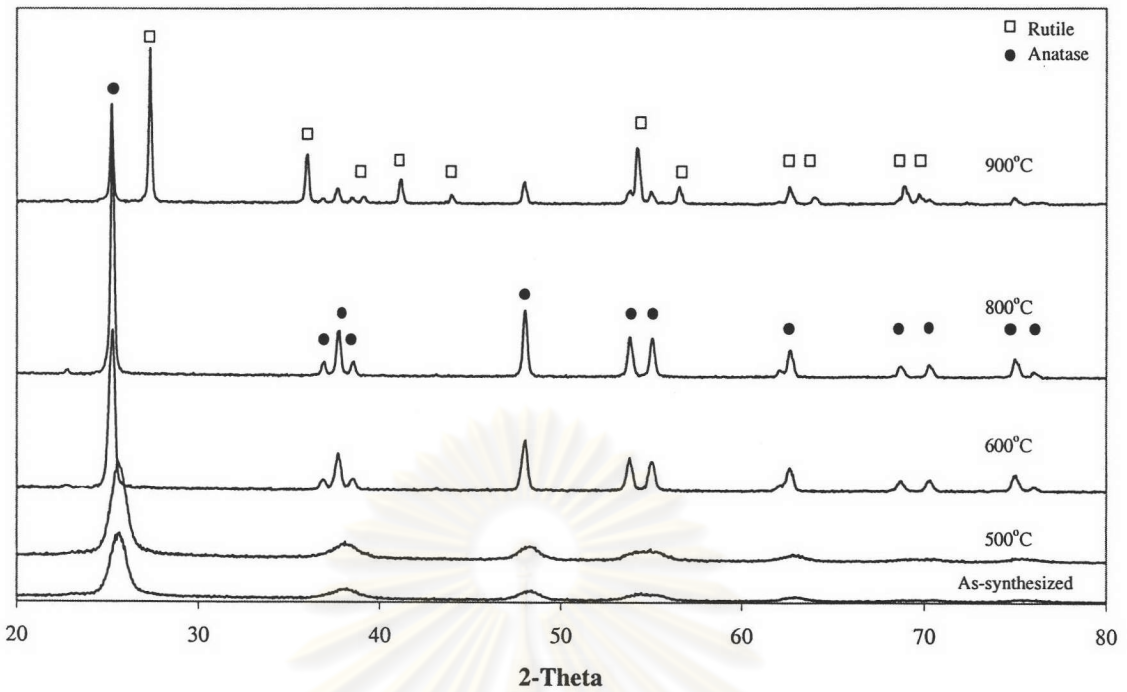

Figure 5.12 XRD pattern of titania products synthesized in 1,4 butanediol at 300°C for 2 hrs and calcined at various temperature.

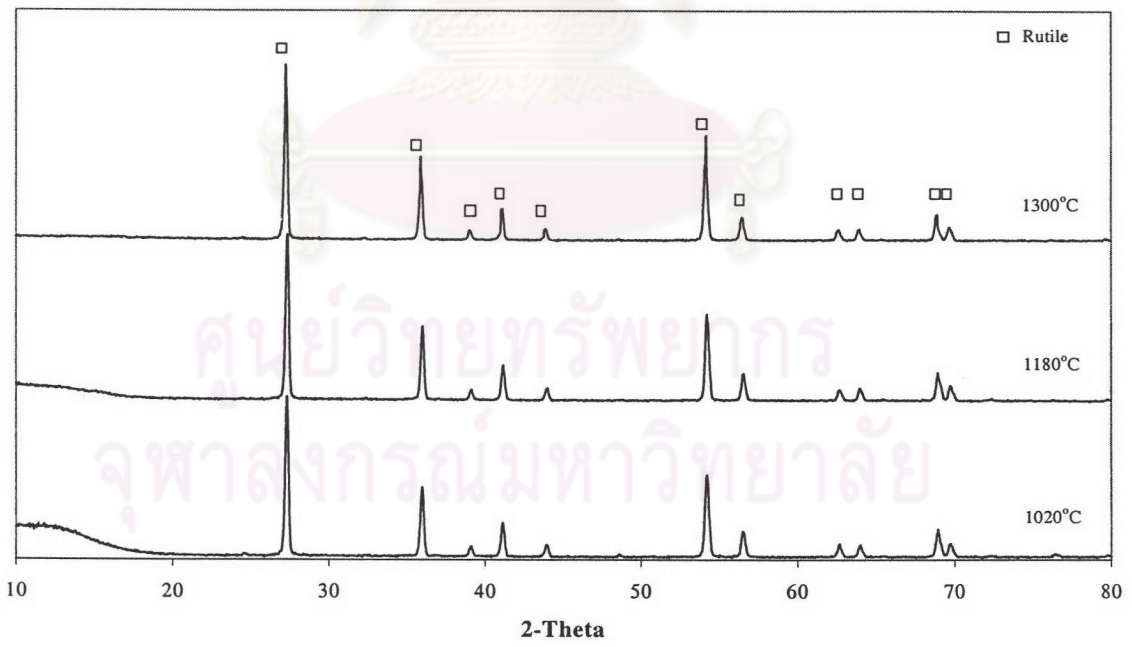

Figure 5.13 XRD pattern of titania products synthesized in 1,4 butanediol calcined at 1020°C for 2 hrs and calcined at various temperature.

The growth rate is given by Eq. (1) (Turnbull, 1956).

$$u = a_0 v_0 \left[\exp\left(-\frac{Q}{KT}\right)\right]\left[1 - \exp\left(-\frac{\Delta Fv}{KT}\right)\right] \quad (1)$$

where a_0 is the particle diameter, v_0 the atomic jump frequency, Q the activation energy for an atom to leave the matrix and attach itself to the growing phase, ΔF_v the molar free energy difference between the two phases. For non-crystallization $\Delta Fv \gg KT$, so Eq. (1) can be reduced to Eq. (2):

$$u = a_0 v_0 \left[\exp\left(-\frac{Q}{KT}\right)\right] \quad (2)$$

When the heating temperature is high, the activation energy is very small, the growth rate is large. So the crystallite size increases very quickly as the increasing heating temperature; when the heating temperature is low, the activation energy is very large, respectively, the growth rate becomes slow. So the crystallite size increases very slowly as the heating temperature increases.

Figure 5.16 shows a set of the typical TEM micrographs of the nano-TiO_2 powders heated at 600 and 1400°C for 2 hr. The effects of heating time on the crystallite size were thought to be controlled mainly by diffusion. At this time the following equation is given (Aaron *et al.*, 1970):

$$u \propto (\alpha Dt)^{1/2} \quad (3)$$

where u is the crystal growth rate, D the diffusion coefficient, t the heating time, α the constant data. Compared with the low heating temperature the diffusion coefficient at high heating temperature is large. Huge driving force for diffusion is present. So the growth rate for the particle is fast at relatively high heating temperatures and the crystallite size tends to change very greatly as the heating time prolong.

But in this study is crystallization. The growth rate u varies with temperature according to an Arrhenius equation.

$$u = u_0 \exp\left(-\frac{Q}{RT}\right) \quad (4)$$

Where R is the gas constant.

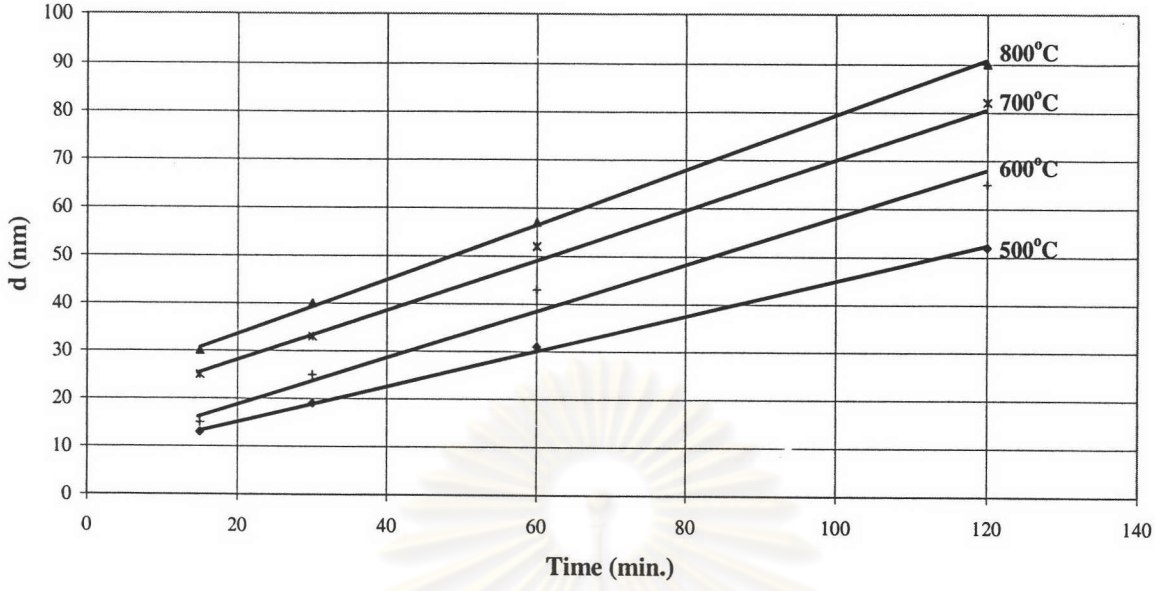

Figure 5.14 The effect of the heating time upon the crystallite size of TiO_2 powders heated at various temperatures in anatase phase.

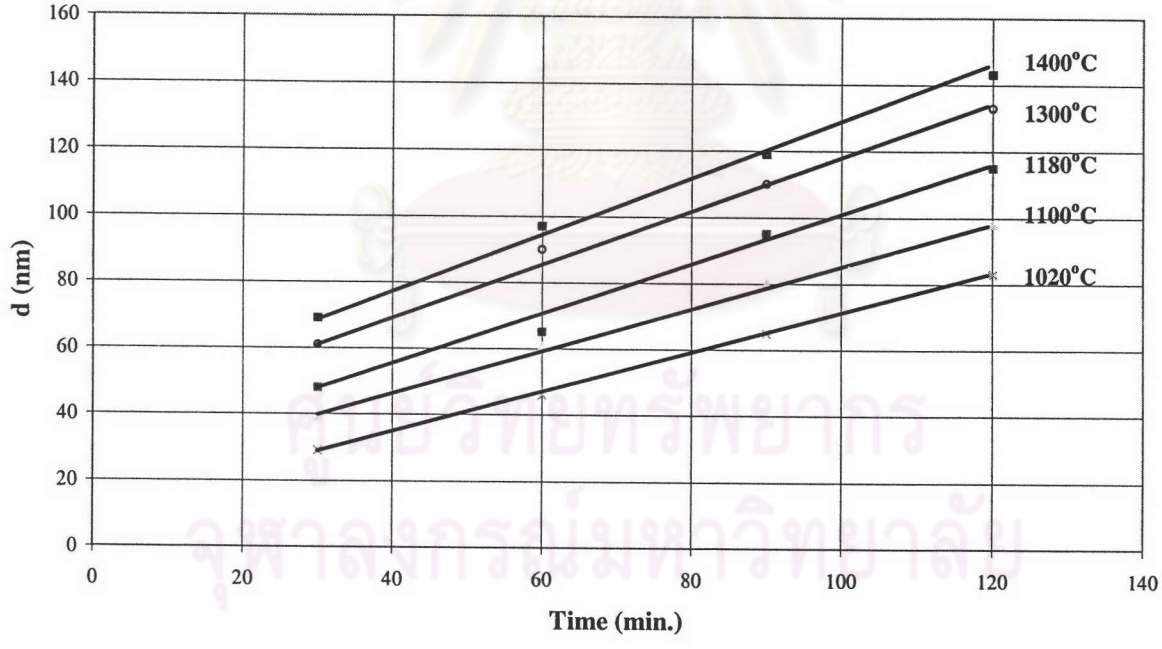

Figure 5.15 The effect of the heating time upon the crystallite size of TiO_2 powders heated at various temperatures in rutile phase.

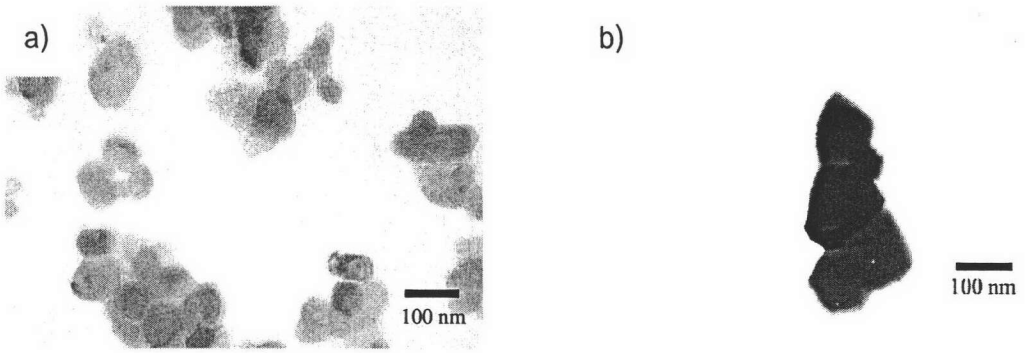

Figure 5.16 TEM micrographs of the nano-TiO_2 powders heated at heating times 2 hr and different heating temperatures: (A) 600; (B) 1400°C.

Table 5.5 The growth rate of TiO_2 in various heating temperature in anatase phase.

Heating temperature (°C)	500	600	700	800
Growth rate	0.3704	0.4684	0.5449	0.5664

Table 5.6 The growth rate of TiO_2 in various heating temperature in rutile phase.

Heating temperature (°C)	1020	1100	1180	1300	1400
Growth rate	0.6033	0.6533	0.7700	0.7867	0.8133

Tables 5.5 and 5.6 showed the growth rate of TiO_2 in various heating temperature. It indicated that growth rate depended on heating temperature. According to the Arrhenius equation, u should increase linearly with exp(1/T). The growth rate of titania particles follow Arrhenius behavior, as shown in Figure 5.17. Activation energies were obtained from the plots shown in Figure 5.17 by the method of least squares.

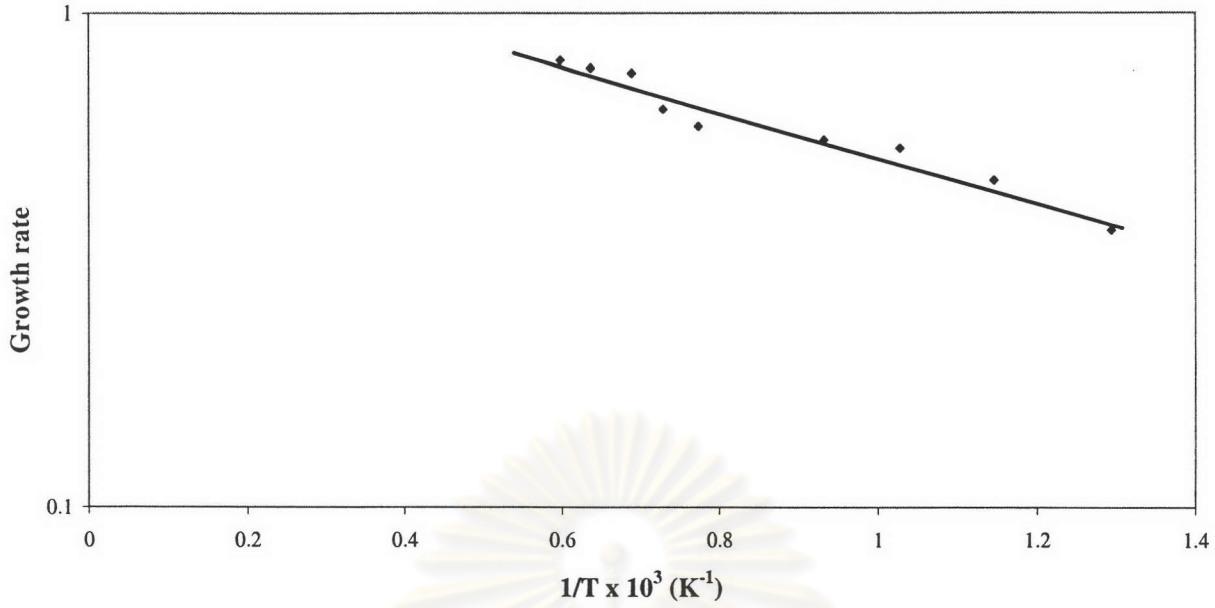

Figure 5.17 Arrhenius plots of the crystal growth of titania.

5.3.2 Synthesized solvents

The effect of the synthesizing solvents upon the crystallite size of TiO_2 powders is shown in Figure 5.18. It was found that the synthesizing solvents at low heating temperatures have not influence on the particle size and growth rate. When the heating temperature increases to 1000°C, the obvious influence on crystallite size was found as same as at low heating temperatures. It concluded that the synthesizing solvents are not effect on crystal growth.

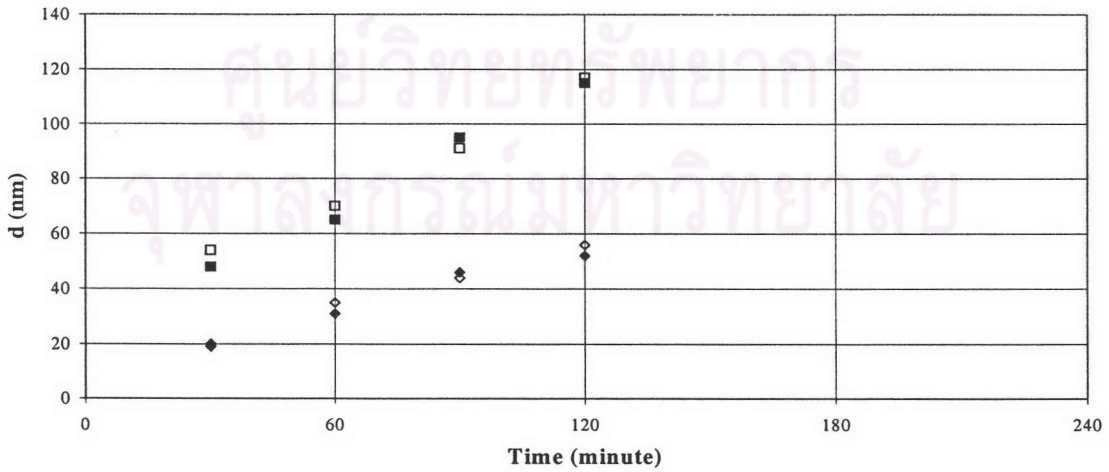

Figure 5.18 The effect of the synthesizing solvents on the crystallite size of TiO_2 powders heated at various temperatures: (♦) 500°C, 1-4-BG (◊) 500°C, toluene (■) 1180°C, 1,4-BG and (□) 1180°C, toluene.